Eddy-induced transport and kinetic energy budget in the Arabian Sea

Item Type	Article
Authors	Zhan, Peng;Guo, Daquan;Hoteit, Ibrahim
Citation	Zhan, P., Guo, D., & Hoteit, I. (2020). Eddy-induced transport and kinetic energy budget in the Arabian Sea. Geophysical Research Letters. doi:10.1029/2020gl090490
Eprint version	Post-print
DOI	10.1029/2020gl090490
Publisher	American Geophysical Union (AGU)
Journal	Geophysical Research Letters
Rights	Archived with thanks to Geophysical Research Letters
Download date	2024-03-13 08:31:11
Link to Item	http://hdl.handle.net/10754/666106

Eddy-induced transport and kinetic energy budget in the Arabian Sea

Peng Zhan[1], Daquan Guo[1], Ibrahim Hoteit[1*]

Corresponding author: Ibrahim Hoteit, Division of Physical Sciences and Engineering, King Abdullah University of Science and Technology, Thuwal, Saudi Arabia. (ibrahim.hoteit@kaust.edu.sa)

[1]Division of Physical Sciences and Engineering, King Abdullah University of Science and Technology, Thuwal, Saudi Arabia.

This study investigates the vertical eddy structure, eddy-induced transport, and eddy kinetic energy (EKE) budget in the Arabian Sea (AS) using an eddy-resolving reanalysis product. The EKE intensifies during summer in the western AS. Anticyclonic eddies (AEs) and cyclonic eddies (CEs) present warm-fresh and cold-salty cores, respectively, with interleaved salinity structures. The eddy-induced swirl transport is larger in the western AS and tends to compensate for heat transport by the mean flow. Zonal drift transport by AEs and CEs offset each other, and meridional transport is generally weaker. Eddies also produce notable upward heat flux during summer in the western AS, where ageostrophic circulations are induced to maintain a turbulent thermal wind balance. Plausible mechanisms for EKE production are governed by baroclinic and barotropic instabilities, which are enhanced in summer in the western basin, where signals are quantitatively one order larger than the turbulent wind inputs.

Key Points

Main point 1: Eddy activities and eddy-induced transport play a crucial role in maintaining oceanic heat and salt conditions in the Arabian Sea.

Main point 2: The western Arabian Sea is identified as a new hotspot in the global ocean with noticeable upward eddy-induced heat transport.

Main point 3: Baroclinic and barotropic instabilities are the primary sources of eddy kinetic energy in the Arabian Sea.

1. Introduction

Mesoscale eddies are one of the key components of circulation [*Fischer et al.*, 2002] and biological processes [*Sergey*, 2012] in the Arabian Sea (AS), particularly in its western basin which exhibit a strong activity similar to that of other eddy-rich regions in the global ocean [*Scharffenberg and Stammer*, 2010; *Roullet et al.*, 2014]. The western AS experiences seasonally reversing monsoonal winds that drive energetic spatiotemporal variability related to the Somali Current (SC), coastal upwelling, and the upper-ocean heat budget [*Schott and McCreary*, 2001; *Fischer et al.*, 2002; *Seo*, 2017; *Wang et al.*, 2018]. Eddy activities also exhibit strong seasonality that peaks during the summer monsoon season [*Trott et al.*, 2018]. Wind stress [*Trott et al.*, 2017], background currents [*Trott et al.*, 2018], and west propagating Rossby waves [*McCreary et al.*, 1993; *Brandt et al.*, 2002] are qualitatively interpreted as possible factors that strengthen eddies in the region; however no consensus has been reached. These eddies drive local upwelling and downwelling [*Trott et al.*, 2019] and could make a large contribution to the marine ecosystem and biogeochemical variability when coupled with wind-induced Ekman pumping [*Seo et al.*, 2008; *Yao and Hoteit*, 2015]. More importantly, eddies transport a significant amount of oceanic properties and influence the spreading pathways of marginal sea water [*Carton et al.*, 2012; *de Marez et al.*, 2019]. In particular, eddies off Somalia cause variabilities in tracers and strongly impact regional transport [*Trott et al.*, 2019], some of which may propagate into the western Gulf of Aden (GoA) and promote the transport of Red Sea water [*Bower and Furey*, 2012].

Transports by mesoscale eddies in oceans play a dominant role in regulating biologi-cal activities [*Chelton et al.*, 2011], general circulation [*Macdonald and Wunsch*, 1996], and regional climate [*Zhang et al.*, 2014]. Eddies induce two types of tracer transport. Swirl transport occurs when the tracer anomalies and rotational velocities are asymmet-ric and, therefore, leads to net transport over the eddy wavelength [*Chelton et al.*, 2011; *Hausmann and Czaja*, 2012]; this process is sometimes enhanced by a series of flanking eddies [*Zhan et al.*, 2016]. Drift transport is caused by the movement of eddies when tracer anomalies inside an eddy are trapped by interior water parcels and move with the eddy [*Dong et al.*, 2014; *Lin et al.*, 2019]. These eddy-induced transports may ex-hibit comparable magnitudes [*Dong et al.*, 2014; *Sun et al.*, 2019], and their contribution should be jointly considered. Estimating eddy-induced transport requires 3D eddy struc-tures, which can be approximated by tracking altimeter maps and simultaneous Argo floats in data-rich regions [*Qiu and Chen*, 2005; *Souza et al.*, 2011; *Chen et al.*, 2012], utilizing a universal structure that is representative of global oceanic mesoscale eddies [*Zhang et al.*, 2013, 2014], or as a more comprehensive alternative, analyzing outputs of an eddy-resolving model [*Volkov et al.*, 2008; *Frenger et al.*, 2015; *Zhan et al.*, 2019].

Previous observational studies provided snapshots of vertical eddy structure at scat-tered locations in the AS [*Fischer et al.*, 2002; *Carton et al.*, 2012; *L'Hegaret et al.*, 2016; *Trott et al.*, 2018]. In a more recent study [*de Marez et al.*, 2019], systematic 3D eddy structures in the northern AS were presented for the first time by a compositing altimeter and Argo data. The aforementioned studies used different types of observations to obtain complementary perspectives, but the spatiotemporal sparseness of the observations pro-

vided only limited understanding of some key features of the AS eddies. In this study, we analyze outputs of the Copernicus Marine Environment Monitoring Service (CMEMS) global eddy-resolving reanalysis product (S1) to explore the 3D eddy structures, quantify and investigate the spatiotemporal characteristics of two types of eddy-induced transport, and further investigate the origins of eddy kinetic energy (EKE) by performing a full EKE budget analysis. This study complements previous knowledge of eddies in the AS and provide comprehensive insights of their transport properties and energy cycle.

2. Eddy kinetic energy

EKE in the AS exhibits pronounced seasonal variability [*Sharma et al.*, 1999]. December to February and June to September are the most representative months under the winter and summer monsoon regimes, respectively [*Beal et al.*, 2013; *Wang et al.*, 2018]. Hereafter, all analyses from the two seasons are extracted from these months. Figure 1 shows the spatial and vertical distributions of seasonally averaged EKE calculated from $EKE = \frac{1}{2}\rho(u'^2 + v'^2)$, where quantities are vertically integrated over the upper 1000 m within which momentum remains active. The wind-induced intraseasonal component of flow variability in the tropical Indian ocean has typical signals between 40 and 100 days [*Han et al.*, 2001; *Han*, 2005]. To eliminate signals at this frequency as well as seasonal variabilities, the primes in EKE denote intraseasonal components of velocities estimated by deviations from a 31-day running mean flow, following a similar approach to that of *Yang et al.* [2013b] and *Chatterjee et al.* [2013].

EKE is mostly confined in the upper 300 m in both seasons and noticeably enhanced east off Somalia during summer, agreeing with the previous studies [*McCreary et al.*, 1993;

87 *Schott and McCreary*, 2001; *Chatterjee et al.*, 2013]. The seasonal surface forcing cycle

88 over the AS drives strong seasonally reversal circulation in western AS [*McCreary et al.*,

89 1993; *Seo et al.*, 2008]: during winter the mean flow is southward along the Somalia coast,

90 whereas the SC intensifies and flows northward under the summer southwest monsoon

91 [*Beal et al.*, 2013] and forms the Great Whirl (GW) with retroflection and structures

92 extending northeast towards the Gulf of Oman (GoO) [*Fischer et al.*, 2002]. EKE in the

93 interior basin is weaker than the western basin, a general trend in world oceans [*Stammer*

94 *and Wunsch*, 1999]. The largest summer EKE appears at $55°E$ and $7°N$, and the most

95 intense signals exceed $5 \times 10^4 J/m^2$. Eddies in the AS propagate westward into the GoA,

96 producing higher EKE during early winter (Figure 1 a) [*Al Saafani et al.*, 2007]. Here,

97 we further verify CMEMS EKE against that calculated using surface geostrophic currents

98 from AVISO data (Figure 1 d and h), which exhibit similar spatiotemporal distributions.

99 A stricter definition to describe the intensity of mesoscale eddies is to estimate their

100 energy from detected individual eddies (S2) as shown in Figure 1 (c) and (g). Such

101 quantity and EKE calculated using the aforementioned mean metric deviations show

102 good agreement, suggesting that EKE is a good approximation of actual mesoscale eddy

103 activities; therefore, the EKE and the associated derivations of energy flux can be used

104 to investigate internal processes and diagnose the energy budget.

105 Nevertheless, some insights of eddy properties still rely on detecting complete eddy

106 fields (Figure 1 i-l). Figure 1 (i) indicates that the majority of eddies are found in the

107 western AS and GoA. Eddies generated in the central AS propagate westward as Rossby

108 waves and accumulate upon reaching the western basin [*Al Saafani et al.*, 2007]. Eddies

can also form locally when the SC flows northward in summer and turns further northeast

in large meanders [*Fischer et al.*, 2002]. The largest and deepest eddies are found in lower

latitudes, particularly the SC region (Figure 1 j and k). A large component is contributed

by the anticyclonic GW developed during the summer monsoon season, which has a radius

and intensity larger than most eddies in the northwestern Indian Ocean [*Trott et al.*, 2018].

The propagation speeds of individual eddies are estimated by tracking their trajectories

in sequential maps (Figure 1 i). Eddies generally move westward and tend to have a

larger speed in the southern basin as they are embedded within the large scale Rossby

waves, which propagate faster in the lower latitudes; though strong background currents

in regions east of the Somalia coast can advect circular eddies along their flow axis.

3. 3D structures of mesoscale eddies

Eddies in the AS show pronounced spatiotemporal variability but tend to exhibit a

uniform structure under normalized coordinates, as reported from a global perspective

[*Zhang et al.*, 2013]. Figure 2 illustrates the generic composite 3D structure of typical

AEs and CEs in the AS with a zonal section across the eddy center. Eddies generally

have maximal subsurface temperature deviations of more than 1.5 ^oC (positive/negative

for AE/CE) ($\sim 120\ m$). Similarly, AE/CE feature negative/positive density anomalies of

approximately 0.3 km/m^3 centered at the same depth. This confirms the previous study

that temperature primarily controls the density structure of eddies in the AS [*Joseph and*

Freeland, 2005] and is consistent with the standard structures in stratified and rotating

flows: AE/CE force isopycnals to sink/rise to create negative/positive density anomalies

[*Vallis*, 2006].

130 Salinity anomalies inside AE/CE are generally negative/positive, yet a layer with an

131 opposite sign appears at the subsurface between 100 and 160 m (i.e., a saltier/fresher

132 layer interrupts the negative/positive salinity anomalies inside the AE/CE), exhibiting a

133 sandwich-like pattern, which was observed by Argo profiles in the region [*de Marez et al.*,

134 2019]. Low salinity water was advected by the Somali and North Equatorial Currents

135 into the AS [*Morrison*, 1997], and high salinity water formed in the northern basin and

136 the Arabian Gulf sinks to the subsurface, yielding a subsurface layer of high salinity

137 water which spreads over a large proportion of the basin [*Rochford*, 1964; *Kumar and*

138 *Prasad*, 1999]. Precipitation and runoff in the eastern AS contribute to the local formation

139 of low salinity waters, which augment the subsurface maximum [*Joseph and Freeland*,

140 2005]. Thus, AE-induced downwelling and CE-induced upwelling synergize an inverse

141 "S" salinity profile structure (Figure 2 f) and create a three-core sandwich-like pattern.

142 Similar prominent salinity profile structures were also reported in the north Pacific [*Qiu*

143 *and Chen*, 2005], the subtropical Pacific [*Yang et al.*, 2013a], and the South China Sea

144 [*Zhang et al.*, 2018].

145 The composite meridional rotational currents are surface-intensified and decreasing with

146 depth. The largest velocities are found at approximately one radius from the eddy center,

147 with maximum azimuthal speeds of more than 0.2 m/s near the surface. Neither the T/S

148 anomalies nor the rotation velocities are symmetric around the eddy core. Such asymme-

149 try is crucial for inducing net swirl transport [*Roemmich and Gilson*, 2001]. AE and CE

150 cause uplift and depression of the background pycnocline profiles, and the associated T/S

151 anomalies with opposite signs could lead to distinct eddy drift transport features.

4. Eddy-induced transport

We first investigate the averaged eddy swirl transport (S2) of heat and salt (Figure 3 a-d). Eddies generally produce stronger swirl transport in the western AS and GoA. Zonally, eddies yield eastward (positive) heat transport in the GoA and east off the Somali Cape towards the GoO. These processes are important for balancing the heat budget and to promote zonal heat exchange between coastal and ambient waters in the region [*Fischer et al.*, 2002; *de Marez et al.*, 2019]. The blue and purple patch east of Somalia (Figure 3 a) suggests strong westward and eastward heat transport with a large zonal temperature gradient persisting, particularly in summer as a result of Ekman pumping effect [*Wilson-Diaz et al.*, 2009; *Trott et al.*, 2017]. Northward (positive) meridional heat transport is found inside the GoA and along a $\sim 100km$ band along the Somalia coast (Figure 3 b); the more pronounced dark blue patch further east suggests large southward heat transport. The northward SC produces strong shear in velocity with its southward retroflection [*Trott et al.*, 2019], generating eddies asymmetry in shape and T/S properties [*Trott et al.*, 2019] and hence inducing intense swirl transport. Eddies in the region induce clockwise patterns of heat transport (indicated by the green arrows in Figure 3 (a, b)), which tends to counteract the transport of upwelled water induced by the Somali cold current and its retroflection [*Fischer et al.*, 2002; *Volkov et al.*, 2008].

Zonal salt transport is positive (eastward) in the GoA, the GoO, and the eastern AS, whereas negative (westward) in the western AS. Precipitation and runoff from rivers in the eastern AS contribute to the local formation of low salinity waters [*Joseph and Free-land*, 2005], and eddy swirl transport tends to decrease the gradient by eastward salt

173 flux. Additionally, high evaporation rates in the northern AS causes high surface salinity

174 [*Morrison*, 1997]. This is compensated by eddy swirl transport with a negative meridional

175 (southward) salt flux in the entire AS and equivalent northward freshwater transport. The

176 only notable exception for meridional salt transport is inside the GoA, where eddies tend

177 to transport saltier water northward.

178   Figure 3 (e-h) shows the averaged drift transport (S3). AEs and CEs normally propa-

179 gate westwards with negative zonal velocities at similar speeds but feature opposite tracer

180 displacement tendencies (Figure 2). Consequently, AEs and CEs produce opposite zonal

181 transports and tend to offset each other; the total transport is smaller than that of either

182 type alone. However, eddies can be coherently advected over regions with strong back-

183 ground currents and produce large drift transport. A typical example is in the western AS

184 off Somalia, where AEs are larger and usually formed by the branches of the background

185 currents (e.g. the GW), while CEs are smaller and more likely to be advected as a well-

186 maintained integral [*Trott et al.*, 2018]. Consequently, the westward propagating cold-core

187 CEs produce positive zonal heat transport (Figure 3 e). The meridional eddy drift trans-

188 port in the interior basin is weak because of limited meridional propagation (Figure 1 i);

189 however, the strong northward SC and southward retroflection can trap and advect eddies

190 in the region (particularly CEs) to form heat transport in the opposite direction (Figure

191 3 f). The drift transport of salt is generally small (Figure 3 g and h), largely because of

192 multi-layer structure in salinity anomaly offset by trap depth integration.

193   From a global perspective, eddy meridional movement tends to transport heat and salt

194 towards the equator in the tropics [*Jayne and Marotzke*, 2002; *Volkov et al.*, 2008]. This

effect is evident in the interior AS, where T/S transports are negative (southward) but not significant. Our analysis suggests that meridional eddy drift transport in the basin is more influenced by background circulation (i.e. the SC and its extension). Meridional eddy drift transport of heat in these regions is at least one order larger than in the interior basin and exhibits patterns consistent with that of background flow.

Total eddy-induced transport is the sum of swirl and drift transport (Figure 3 i-p). Swirl transport generally exhibits larger magnitude, and the two types of transport have the same order and may synergize or compensate each other depending on location. As reported by *Hastenrath and Greischar* [1993]; *Wilson-Diaz et al.* [2009], the oceanic heat transport to the AS switches between seasons (northward in winter while southward in summer). The annual average of heat transport is $\sim 105 TW$ across the $6\,°N$ section, out of which about 15 % ($\sim 16 TW$) is contributed by eddies that transport heat southward throughout the year. Positive zonal T/S transport within the GoA suggests that eddies transport cooler, fresher water to the western end of the GoA, a process that actively spreads Red Sea outflow and generates large T/S gradients to form favorable conditions for fingering and diffusive convection [*Bower and Furey*, 2012]. Positive meridional heat transport in the gulf further suggests that eddies are important transporters of warmer water towards the northern coast and moderators of the summer Ekman upwelled thermocline [*Yao and Hoteit*, 2015]. Eddies also transport warmer, saltier water outflow from the Arabian Gulf eastward into GoO, as evidenced by in-situ observations [*L'Hegaret et al.*, 2016].

216   Additionally, SST data indicate that eddies may sometimes transport coastal upwelled

217 water offshore of Somalia with filament structures on the surface [*Fischer et al.*, 2002]. A

218 close-up of the cross section reveals similar statistical features with negative zonal heat

219 transport in the uppermost layers (Figure 3 m, equivalent to eastward transport of colder

220 water). However, the larger heat flux is contributed by the subsurface layer where heat

221 is transported in the opposite direction. Eddies in the SC region generally have deeper

222 structures than those of the interior basin and have deeper penetration cores between 100-

223 200 m. In the meridional direction, eddies transport heat northward in the upper layers,

224 whereas thicker deeper layers produce southward heat transport with maximal values at

225 $\sim 180 \ m$.

Furthermore, circulation is not fully aligned with the isothermal, and it is the cross-isothermal component that directly contributes to heat exchange between water parcels. We estimated the cross-isothermal heat transport of mean flow and eddy flow by projecting their velocities onto the direction of temperature gradient, i.e.,

$$Q_{heat,cross-iso} = \rho C_p T \mathbf{u_h} \cdot (\nabla_h T / |\nabla_h T|).$$

The basin-integrated $Q_{heat,cross-iso}$ by mean flow is down-gradient (from warmer to colder water) in winter while up-gradient (from colder to warmer water) in summer. The variability offsets between seasons and yields an annual average of $\sim 2.1 PW$ up-gradient transport integrated over the entire AS. In contrast, this is over-compensated by the eddy-induced $Q_{heat,cross-iso}$, which is dominantly down-gradient all over the year with an annual average of $\sim 5.2 PW$. This agrees with the general Fickian-like form hypothesis [*Stammer*, 1998] where eddy transport is assumed down-gradient, and it can be explained by diagnosing

DRAFT   November 13, 2020, 5:28am   DRAFT

the baroclinic energy conversion [*Brooks and Niiler*, 1977; *Jayne and Marotzke*, 2002]

$$-\overline{\rho'w'}g = \frac{g}{|\partial\bar{\rho}/\partial z|}\left(\overline{\rho'u'}\frac{\partial\bar{\rho}}{\partial x} + \overline{\rho'v'}\frac{\partial\bar{\rho}}{\partial y}\right),$$

which, if neglecting the salinity effect under reasonably constant stratification, reduces to

$$-\overline{T'\mathbf{u_h'}} \cdot (\nabla_h\overline{T}).$$

This suggests that eddies tend to transport heat down-gradient when baroclinic energy is converted from mean flow to eddy fields $(-\overline{\rho'w'}g > 0)$, which is proved true for the AS as discussed in the next section. Following a similar approach, we estimate the cross-isosaline transport using

$$Q_{salt,cross-iso} = \rho S\mathbf{u_h} \cdot (\nabla_h S/|\nabla_h T|).$$

226 Our analysis indicates that both mean and eddy flow in the AS produce down-gradient

227 cross-isosaline transport, in which eddies contribute $2.4 \times 10^9 kg/s$, accounting for about

228 19% of the total transport in the entire AS. Although gradients in T/S have an opposite

229 effect on density gradient, it is not surprising that eddy-induced cross-isosaline transport

230 is also down-gradient, since it is temperature that has a dominant control on the den-

231 sity structure in the AS [*Joseph and Freeland*, 2005], and hence the baroclinic energy

232 production as discussed above.

233   It is worth noting that eddies also induce noticeable vertical transport, particularly

234 during summer in the western AS (Figure 4). Other regions with intense vertical eddy

235 transport distribute near warm western boundary current extensions, e.g., the Kuroshio,

236 Gulf Stream, and Agulhas Return Current, where eddies transport heat upward, com-

237 pensating intense surface cooling [*Vivier et al.*, 2002; *Dong and Kelly*, 2004; *Yang et al.*,

238 2016]. However, the AS is featured with unique dynamics different from all these above:

239 the poleward SC is a cold boundary current due to Ekman effect [*Wilson-Diaz et al.*, 2009;

240 *Wang et al.*, 2018]. Among different atmospheric forcings, it is the monsoon momentum

241 flux (Figure 4 j) that drives the SC, strong upwelling and vigorous turbulent mixing dur-

242 ing summer [*Beal et al.*, 2013; *Trott et al.*, 2017], coinciding with the period when eddies

243 are enhanced in this region (Section 3). This makes flows of mesoscale eddies subject

244 to the turbulent thermal wind (TTW) balance (the balance between the Coriolis force,

245 horizontal pressure gradient, and vertical mixing of momentum) [*Gula et al.*, 2014]. The

246 turbulent mixing would destruct vertical shear in eddies, consequently, an ageostrophic

247 secondary circulation is induced to restore the vertical shear and maintain the TTW bal-

248 ance [*Gula et al.*, 2014; *Jing et al.*, 2020]. It has been proved that such processes convert

249 eddy potential energy to EKE and generate upward eddy heat transport in the mixed

250 layer [*Jing et al.*, 2020]. Our analysis gives evidence of this mechanism in the western AS,

251 as shown in Figure 4 (h), where the dark purple patch indicates stronger ageostrophic

252 circulations east of Somalia coast in summer, coinciding with the regions of larger eddy

253 vertical transport (Figure 4 f and g) and higher EKE (Figure 1 e). This area is much

254 larger than the coastal region where seasonally averaged flow upwells (Figure 4 i). The

255 offshore Ekman transport tends to spread and disperse the cold water into the open basin,

256 while the eddy-induced heat flux is upward of comparable magnitude to the net heat gain

257 at the surface (not shown), suggesting the fundamental role of oceanic eddies in main-

258 taining the fronts. In total, eddies induce upward heat transport of about 22 TW across

259 65 m in the AS, offsetting about 30% of the downward heat transport by mean flow.

260 In general, eddies act as an important heat supplier to the upper ocean in the western

261 AS, particularly during summer. Meanwhile, eddy-induced vertical salt fluxes exhibit a

262 seasonal variability that is downward during winter and upward during summer (Figure 4

263 b and g). The annual average is downward of $\sim 3.7 \times 10^5 kg/s$, accounting for only $\sim 3\%$

264 of the total downward salt transport.

5. Origins of Eddy Kinetic Energy

265 We further investigate the origins of EKE in the AS by diagnosing the complete 3D

266 energy budget (S4), with a particular focus on eddy energy generation. Obvious differences

267 are discernible among the energy flux terms between winter and summer corresponding

268 to seasonal EKE variability (Figure 5). The ubiquitously positive values of T1 ($-\overline{\rho' w' g}$)

269 suggest that eddy potential energy is released via baroclinic instability across the AS

270 (necessary conditions for baroclinic instability are satisfied, not shown). In particular,

271 maximal values were identified east of Somalia in summer (1st column of Figure 5), when

272 the strong southwesterly monsoon causes upwelling along the Somalia coast. The uplifted

273 isopycnal is tilted downslope towards the east (Figure 5 t), preconditioning baroclinic

274 instability that peaks from 50-180 m. This term usually follows the location of the mean

275 lateral density gradients, as expected from the linear instability theory [$Green$, 1970]. The

276 pycnocline is flatter in the interior basin, particularly in winter, and therefore limits EKE

277 production.

278 Another source term, T5 ($\rho_0 \overline{\mathbf{u}'_h \cdot (\mathbf{u}' \cdot \nabla \overline{\mathbf{u}_h})}$), presents larger amplitudes in summer east

279 of Somalia (2nd column of Figure 5). Positive T5 implies KE transfer from mean flow to

280 eddies, agreeing with the analysis of EKE associated with the Southern Gyre [$Chatterjee$

281 $et\ al.$, 2013]. The large horizontal velocity shear in summer enhances barotropic instability,

282 with a larger magnitude than T1 and extends further east. A blue patch between the SC

283 and its retroflection suggests that eddies can feed energy back into the SC at a thin band.

284 In winter, mean circulations in the western AS tend to convert MKE into EKE yet at a

285 much smaller rate than in summer, since the shear of horizontal velocity is much weaker

286 which limits the development of barotropic instability.

287 T2 $(-\frac{\partial \overline{p'w'}}{\partial z})$, T3 $(-\nabla_h \cdot \overline{p'\mathbf{u}'_h})$, and T4 $(-\frac{\rho_0}{2}\nabla \cdot \overline{(\mathbf{u} \cdot \mathbf{u}'^2_h)})$ are EKE redistribution terms

288 by vertical pressure work, horizontal pressure work, and advection, respectively (3rd and

289 4th column of Figure 5). Similarly, these terms are more amplified in summer in the

290 western AS. T2 is mixed with upward and downward flux above and below the pycno-

291 cline, respectively. This divergence suggests that EKE generated at the subsurface are

292 propagated upward towards the surface and downward towards deeper layers. EKE is

293 locally exchanged with ambient water through horizontal pressure work and advection.

294 In particular, along the axis of the SC and its retroflection, EKE is rapidly spread by

295 T3 and T4, agreeing with EKE production by T5 that is maximized along the flow axis

296 (Figure 5 q). In the western AS and the GoA, speckled blue and red patches of T3 and

297 T4 indicate the rapid divergence/convergence of horizontal eddy energy fluxes, whereas

298 signals in the interior basin are much weaker. This is because the eddies produce limited

299 net horizontal energy flux while propagating westward as Rossby waves in the interior AS

300 but tend to actively exchange their energy with ambient water upon reaching the western

301 basin [*Al Saafani et al.*, 2007; *Wang et al.*, 2018].

302 Eddies are reportedly generated as a response to monsoonal forcing on surface current

303 variability [*Fischer et al.*, 2002; *Trott et al.*, 2017]. Our analysis confirms this, with the

304 direct generation of EKE through turbulent wind being positive in the entire AS (Figure

305 5 e and j). This agrees with global open oceans [*Von Storch et al.*, 2012] and other

306 marginal seas [*Pujol and Larnicol*, 2005; *Chen et al.*, 2009; *Zhan et al.*, 2018; *Chen et al.*,

307 2016, 2018], yet the magnitude over the AS is about one order smaller than major regions

308 of high EKE as discussed above. Meanwhile, although the eastern basin exhibits much

309 weaker EKE, more than 50% of which is contributed by the direct wind stress, making it

310 the primary energy source over the large eastern basin. In comparison, winds' contribution

311 is one order smaller than the oceanic internal instabilities in the SC region, particularly

312 during summer.

313   Furthermore, to compare the EKE production at different geographic locations, the AS

314 is divided into five sub-regions as shown in Figure 5 (u), where A, B, C, D, E respond

315 to the Gulf of Aden, Gulf of Oman, northwestern AS, southwestern AS, and eastern

316 AS, respectively. The corresponding domain averaged EKE flux terms are illustrated in

317 Figure 5 (v) for winter and (w) for summer (note difference in their vertical scales). During

318 winter, the EKE is predominantly produced by baroclinic instability and wind stress across

319 the entire AS, with those in the western basin two times larger than the eastern basin.

320 During summer, the southwestern AS (sub-region D) is noticeably distinguished by the

321 elevated EKE production rate about five times higher than others, primarily contributed

322 by barotropic and baroclinic instabilities, while the EKE sources in the other sub-regions

323 are attributed by baroclinic instability and wind at a similar level. In both seasons, the

324 negative values of T2 and T3+T4 suggest that EKE propagates into deep ocean and more

325 significantly, into coastal (shallower) regions.

6. Summary

Most previous studies for the AS concentrate on larger-scale circulations or particular eddies, using sparse observations or coarser-resolution models. In this study we focused on an unexplored aspect that was poorly understood before, the spacial-temporal variability of eddy-induced transport and eddy energy budget, based on a high-resolution global reanalysis product. In addition, this study identifies one new hotspot in the global ocean with noticeable upward eddy-induced heat transport, and offers a new perspective on the dynamics sustaining the SST fronts in the western AS during summer.

The AS exhibits pronounced intraseasonal and spatial variability in eddy activity. Elevated EKE exhibits during summer, primarily east of the Somalia coast. Composite maps show AE/CE can induce warm/cold temperature anomalies with an intensified subsurface magnitude where a single-core appears at approximately 100 m. Salinity anomalies are intensified at the surface with an interleaved sandwich-like structure. Eddies-induce swirl and drift transports are estimated based on detected individual eddies and their tracks. The analysis of a complete heat/salt budget is beyond the scope of this study, but important insights are gained by investigating the horizontal and vertical T/S transport due to mecoscale eddies, which is a key component that modulates the heat and salt content in the western AS. In general, eddy currents affect flux of heat more than salt. The swirl component was generally larger than the drift component in the west AS, yet their magnitude are comparable in the interior basin. The overall cross-iso eddy-induced T/S transports in the AS are both down-gradient, in which the total cross-isothermal transport of mean flow is over compensated by eddies. Eddies also produce vertical heat and

salt supply to the upper ocean in the western AS through the TTW balance mechanism, and the western AS is identified to be a new hotspot in the global ocean with noticeable upward eddy-induced heat transport. This transports are primarily confined to the upper $300\,m$ during summer. The results of this study provide detailed spatiotemporal estimates by accounting for simultaneous fields of individual eddies and small or short-lived eddies not detectable with altimetry and binning Argo data from a global perspective [*Zhang et al.*, 2014; *Dong et al.*, 2014; *Sun et al.*, 2019]. This is particularly important when westward-propagating eddies impale themselves on the high ridges flanking other eddies [*Bower and Furey*, 2012].

In the global ocean, major hot spots of high EKE usually cooccur with intrusion of warm subtropical western boundary current into the cold subpolar ocean. In these regions, intense horizontal gradient in density and strong velocity shear generate respectively the baroclinic and barotropic instabilities that further form a large amount of mecoscale eddies. In this respect, the western AS is unique with the cold Somali boundary current prevails during summer due to Ekman pumping at coast, and the upwelled cold water intrudes into the warmer water in the western AS. Despite such differences, the strong cold Somali current can still precondition baroclinic and barotropic instabilities that predominantly produce of EKE, through which energy from large-scale circulation is converted to mesoscale eddies. The maximum EKE production appears in the subsurface layers, and vertical eddy energy fluxes reconcile the mismatch between the depth of EKE production and eddy activity at upper or lower layers. Direct turbulent wind power input is positive in the interior AS yet weaker than internal instability production in the western basin.

Stronger power input is produced from time-mean winds and circulation [*Von Storch et al.*, 2012], and the net conversion from MKE to EKE indicates a power pathway from winds to time-mean circulation and, eventually, to time-varying eddy circulation.

—————————————————————————————

References

Al Saafani, M. A., S. S. Shenoi, D. Shankar, M. Aparna, J. Kurian, F. Durand, and P. N. Vinayachandran (2007), Westward movement of eddies into the Gulf of Aden from the Arabian Sea, *Journal of Geophysical Research: Oceans*, doi:10.1029/2006JC004020.

Beal, L. M., V. Hormann, R. Lumpkin, and G. R. Foltz (2013), The response of the surface circulation of the arabian sea to monsoonal forcing, *Journal of Physical Oceanography*, doi:10.1175/JPO-D-13-033.1.

Bower, A. S., and H. H. Furey (2012), Mesoscale eddies in the Gulf of Aden and their impact on the spreading of Red Sea Outflow Water, *Progress in Oceanography*, doi: 10.1016/j.pocean.2011.09.003.

Brandt, P., L. Stramma, F. Schott, J. Fischer, M. Dengler, and D. Quadfasel (2002), Annual Rossby waves in the Arabian Sea from TOPEX/POSEIDON altimeter and in situ data, *Deep-Sea Research Part II: Topical Studies in Oceanography*, doi:10.1016/S0967-0645(01)00166-7.

Brooks, I. H., and P. P. Niiler (1977), ENERGETICS OF THE FLORIDA CURRENT., *Journal of Marine Research*.

Carton, X., P. L'Hegaret, and R. Baraille (2012), Mesoscale variability of water masses in the Arabian Sea as revealed by ARGO floats, *Ocean Science*, doi:10.5194/os-8-227-2012.

Chatterjee, A., D. Shankar, J. P. McCreary, and P. N. Vinayachandran (2013), Yanai waves in the western equatorial Indian Ocean, *Journal of Geophysical Research: Oceans*, doi:10.1002/jgrc.20121.

Chelton, D. B., P. Gaube, M. G. Schlax, J. J. Early, and R. M. Samelson (2011), The influence of nonlinear mesoscale eddies on near-surface oceanic chlorophyll, *Science*, doi:10.1126/science.1208897.

Chen, G., Y. Hou, X. Chu, P. Qi, and P. Hu (2009), The variability of eddy kinetic energy in the South China Sea deduced from satellite altimeter data, *Chinese Journal of Oceanology and Limnology*, doi:10.1007/s00343-009-9297-6.

Chen, G., J. Gan, Q. Xie, X. Chu, D. Wang, and Y. Hou (2012), Eddy heat and salt transports in the South China Sea and their seasonal modulations, *Journal of Geophysical Research: Oceans*, doi:10.1029/2011JC007724.

Chen, G., W. Han, Y. Li, and D. Wang (2016), Interannual variability of equatorial eastern Indian Ocean upwelling: Local versus remote forcing, *Journal of Physical Oceanography*, doi:10.1175/JPO-D-15-0117.1.

Chen, G., Y. Li, Q. Xie, and D. Wang (2018), Origins of Eddy Kinetic Energy in the Bay of Bengal, *Journal of Geophysical Research: Oceans*, doi:10.1002/2017JC013455.

de Marez, C., P. L'Hégaret, M. Morvan, and X. Carton (2019), On the 3D structure of eddies in the Arabian Sea, *Deep-Sea Research Part I: Oceanographic Research Papers*, doi:10.1016/j.dsr.2019.06.003.

Dong, C., J. C. McWilliams, Y. Liu, and D. Chen (2014), Global heat and salt transports by eddy movement, *Nature Communications*, doi:10.1038/ncomms4294.

Dong, S., and K. A. Kelly (2004), Heat budget in the Gulf Stream region: The importance of heat storage and advection, *Journal of Physical Oceanography*, doi:10.1175/1520-0485(2004)034¡1214:HBITGS¿2.0.CO;2.

Fischer, A. S., R. A. Weller, D. L. Rudnick, C. C. Eriksen, C. M. Lee, K. H. Brink, C. A. Fox, and R. R. Leben (2002), Mesoscale eddies, coastal upwelling, and the upper-ocean heat budget in the Arabian Sea, *Deep-Sea Research Part II: Topical Studies in Oceanography*, doi:10.1016/S0967-0645(02)00036-X.

Frenger, I., M. Münnich, N. Gruber, and R. Knutti (2015), Southern Ocean eddy phenomenology, *Journal of Geophysical Research: Oceans*, doi:10.1002/2015JC011047.

Green, J. S. (1970), Transfer properties of the largescale eddies and the general circulation of the atmosphere, *Quarterly Journal of the Royal Meteorological Society*, doi:10.1002/qj.49709640802.

Gula, J., J. J. Molemaker, and J. C. Mcwilliams (2014), Submesoscale cold filaments in the Gulf Stream, *Journal of Physical Oceanography*, doi:10.1175/JPO-D-14-0029.1.

Han, W. (2005), Origins and dynamics of the 90-day and 30-60-day variations in the equatorial Indian Ocean, *Journal of Physical Oceanography*, doi:10.1175/JPO2725.1.

Han, W., D. M. Lawrence, and P. J. Webster (2001), Dynamical response of equatorial Indian Ocean to intraseasonal winds: Zonal flow, *Geophysical Research Letters*, doi:10.1029/2001GL013701.

Hastenrath, S., and L. Greischar (1993), The monsoonal heat budget of the hydrosphere-atmosphere system in the Indian Ocean sector, *Journal of Geophysical Research*, doi:10.1029/92jc02956.

Hausmann, U., and A. Czaja (2012), The observed signature of mesoscale eddies in sea surface temperature and the associated heat transport, *Deep-Sea Research Part I: Oceanographic Research Papers*, doi:10.1016/j.dsr.2012.08.005.

Jayne, S. R., and J. Marotzke (2002), The oceanic eddy heat transport, *Journal of Physical Oceanography*, doi:10.1175/1520-0485(2002)032¡3328:TOEHT¿2.0.CO;2.

Jing, Z., S. Wang, L. Wu, P. Chang, Q. Zhang, B. Sun, X. Ma, B. Qiu, J. Small, F.-F. Jin, Z. Chen, B. Gan, Y. Yang, H. Yang, and X. Wan (2020), Maintenance of mid-latitude oceanic fronts by mesoscale eddies, *Science Advances*, *6*(31), eaba7880, doi:10.1126/sciadv.aba7880.

Joseph, S., and H. J. Freeland (2005), Salinity variability in the Arabian Sea, *Geophysical Research Letters*, doi:10.1029/2005GL022972.

Kumar, S. P., and T. G. Prasad (1999), Formation and spreading of Arabian Sea high-salinity water mass, *Journal of Geophysical Research: Oceans*, doi:10.1029/1998jc900022.

L'Hegaret, P., X. Carton, S. Louazel, and G. Boutin (2016), Mesoscale eddies and submesoscale structures of Persian Gulf Water off the Omani coast in spring 2011, *Ocean Science*, doi:10.5194/os-12-687-2016.

Lin, X., Y. Qiu, and D. Sun (2019), Thermohaline Structures and Heat/Freshwater Transports of Mesoscale Eddies in the Bay of Bengal Observed by Argo and Satellite Data, doi:10.3390/rs11242989.

Macdonald, A. M., and C. Wunsch (1996), An estimate of global ocean circulation and heat fluxes, *Nature*, doi:10.1038/382436a0.

McCreary, J. P., P. K. Kundu, and R. L. Molinari (1993), A numerical investigation of dynamics, thermodynamics and mixed-layer processes in the Indian Ocean, doi:10.1016/0079-6611(93)90002-U.

Morrison, J. M. (1997), Inter-monsoonal changes in the T-S properties of the near-surface waters of the northern Arabian Sea, *Geophysical Research Letters*, doi: 10.1029/97GL01876.

Pujol, M. I., and G. Larnicol (2005), Mediterranean sea eddy kinetic energy variability from 11 years of altimetric data, *Journal of Marine Systems*, doi: 10.1016/j.jmarsys.2005.07.005.

Qiu, B., and S. Chen (2005), Eddy-induced heat transport in the subtropical North Pacific from Argo, TMI, and altimetry measurements, *Journal of Physical Oceanography*, doi: 10.1175/JPO2696.1.

Rochford, D. J. (1964), Salinity maxima in the upper 1000 metres of the north Indian ocean, *Marine and Freshwater Research*, doi:10.1071/MF9640001.

Roemmich, D., and J. Gilson (2001), Eddy transport of heat and thermocline waters in the North Pacific: A key to interannual/decadal climate variability?, *Journal of Physical Oceanography*, doi:10.1175/1520-0485(2001)031¡0675:ETOHAT¿2.0.CO;2.

Roullet, G., X. Capet, and G. Maze (2014), Global interior eddy available potential energy diagnosed from Argo floats, *Geophysical Research Letters*, doi:10.1002/2013GL059004.

Scharffenberg, M. G., and D. Stammer (2010), Seasonal variations of the large-scale geostrophic flow field and eddy kinetic energy inferred from the TOPEX/Poseidon and Jason-1 tandem mission data, *Journal of Geophysical Research: Oceans*, doi: 10.1029/2008JC005242.

Schott, F. A., and J. P. McCreary (2001), The monsoon circulation of the Indian Ocean, doi:10.1016/S0079-6611(01)00083-0.

Seo, H. (2017), Distinct influence of air-sea interactions mediated by mesoscale sea surface temperature and surface current in the Arabian Sea, *Journal of Climate*, doi: 10.1175/JCLI-D-16-0834.1.

Seo, H., R. Murtugudde, M. Jochum, and A. J. Miller (2008), Modeling of mesoscale coupled ocean-atmosphere interaction and its feedback to ocean in the western Arabian Sea, *Ocean Modelling*, doi:10.1016/j.ocemod.2008.07.003.

Sergey, P. (2012), Mesoscale Eddies of Arabian Sea: Physical-biological Interactions, *International Journal of Marine Science*, doi:10.5376/ijms.2012.02.0007.

Sharma, R., A. K. Gopalan, and M. M. Ali (1999), Interannual variation of eddy kinetic energy from topex altimeter observations, *Marine Geodesy*, doi:10.1080/014904199273371.

Souza, J. M., C. De Boyer Montégut, C. Cabanes, and P. Klein (2011), Estimation of the Agulhas ring impacts on meridional heat fluxes and transport using ARGO floats and satellite data, *Geophysical Research Letters*, doi:10.1029/2011GL049359.

Stammer, D. (1998), On eddy characteristics, eddy transports, and mean flow properties, *Journal of Physical Oceanography*, doi:10.1175/1520-0485(1998)028¡0727:OECETA¿2.0.CO;2.

Stammer, D., and C. Wunsch (1999), Temporal changes in eddy energy of the oceans, *Deep-Sea Research Part II: Topical Studies in Oceanography*, doi:10.1016/S0967-0645(98)00106-4.

Sun, B., C. Liu, and F. Wang (2019), Global meridional eddy heat transport inferred from Argo and altimetry observations, *Scientific Reports*, doi:10.1038/s41598-018-38069-2.

Trott, C. B., B. Subrahmanyam, and V. S. Murty (2017), Variability of the Somali Current and eddies during the southwest monsoon regimes, *Dynamics of Atmospheres and Oceans*, doi:10.1016/j.dynatmoce.2017.07.002.

Trott, C. B., B. Subrahmanyam, A. Chaigneau, and T. Delcroix (2018), Eddy Tracking in the Northwestern Indian Ocean During Southwest Monsoon Regimes, *Geophysical Research Letters*, doi:10.1029/2018GL078381.

Trott, C. B., B. Subrahmanyam, A. Chaigneau, and H. L. Roman-Stork (2019), Eddy-Induced Temperature and Salinity Variability in the Arabian Sea, *Geophysical Research Letters*, doi:10.1029/2018GL081605.

Vallis, G. K. (2006), *Atmospheric and Oceanic Fluid Dynamics*, doi:10.1017/cbo9780511790447.

Vivier, F., K. A. Kelly, and L. A. Thompson (2002), Heat budget in the Kuroshio extension region: 1993-99, *Journal of Physical Oceanography*, doi:10.1175/1520-0485(2002)032¡3436:HBITKE¿2.0.CO;2.

Volkov, D. L., T. Lee, and L. L. Fu (2008), Eddy-induced meridional heat transport in the ocean, *Geophysical Research Letters*, doi:10.1029/2008GL035490.

Von Storch, J. S., C. Eden, I. Fast, H. Haak, D. Hernández-Deckers, E. Maier-Reimer, J. Marotzke, and D. Stammer (2012), An estimate of the Lorenz energy cycle for the World Ocean based on the 1/10°STORM/NCEP simulation, *Journal of Physical Oceanography*, doi:10.1175/JPO-D-12-079.1.

Wang, H., J. L. McClean, L. D. Talley, and S. Yeager (2018), Seasonal Cycle and Annual Reversal of the Somali Current in an Eddy-Resolving Global Ocean Model, *Journal of*

533 *Geophysical Research: Oceans*, doi:10.1029/2018JC013975.

534 Wilson-Diaz, D., A. J. Mariano, and R. H. Evans (2009), On the heat budget of

535 the Arabian Sea, *Deep-Sea Research Part I: Oceanographic Research Papers*, doi:

536 10.1016/j.dsr.2008.09.003.

537 Yang, G., F. Wang, Y. Li, and P. Lin (2013a), Mesoscale eddies in the northwestern

538 subtropical Pacific Ocean: Statistical characteristics and three-dimensional structures,

539 *Journal of Geophysical Research: Oceans*, doi:10.1002/jgrc.20164.

540 Yang, H., L. Wu, H. Liu, and Y. Yu (2013b), Eddy energy sources and sinks in the

541 South China Sea, *Journal of Geophysical Research: Oceans*, *118*(9), 4716–4726, doi:

542 10.1002/jgrc.20343.

543 Yang, H., J. Liu, G. Lohmann, X. Shi, Y. Hu, and X. Chen (2016), Ocean-atmosphere

544 dynamics changes associated with prominent ocean surface turbulent heat fluxes trends

545 during 19582013, *Ocean Dynamics*, doi:10.1007/s10236-016-0925-3.

546 Yao, F., and I. Hoteit (2015), Thermocline regulated seasonal evolution of surface chloro-

547 phyll in the Gulf of Aden, *PLoS ONE*, doi:10.1371/journal.pone.0119951.

548 Zhan, P., A. C. Subramanian, F. Yao, A. R. Kartadikaria, D. Guo, and I. Hoteit (2016),

549 The eddy kinetic energy budget in the Red Sea, *Journal of Geophysical Research:*

550 *Oceans*, *121*(7), 4732–4747, doi:10.1002/2015JC011589.

551 Zhan, P., G. Gopalakrishnan, A. C. Subramanian, D. Guo, and I. Hoteit (2018), Sensitivity

552 Studies of the Red Sea Eddies Using Adjoint Method, *Journal of Geophysical Research:*

553 *Oceans*, *0*(ja), doi:10.1029/2018JC014531.

Zhan, P., G. Krokos, D. Guo, and I. Hoteit (2019), Three-Dimensional Signature of the Red Sea Eddies and Eddy-Induced Transport, *Geophysical Research Letters*, doi: 10.1029/2018GL081387.

Zhang, W. Z., Q. Ni, and H. Xue (2018), Composite eddy structures on both sides of the Luzon Strait and influence factors, *Ocean Dynamics*, doi:10.1007/s10236-018-1207-z.

Zhang, Z., Y. Zhang, W. Wang, and R. X. Huang (2013), Universal structure of mesoscale eddies in the ocean, *Geophysical Research Letters*, doi:10.1002/grl.50736.

Zhang, Z., W. Wang, and B. Qiu (2014), Oceanic mass transport by mesoscale eddies, *Science*, doi:10.1126/science.1252418.
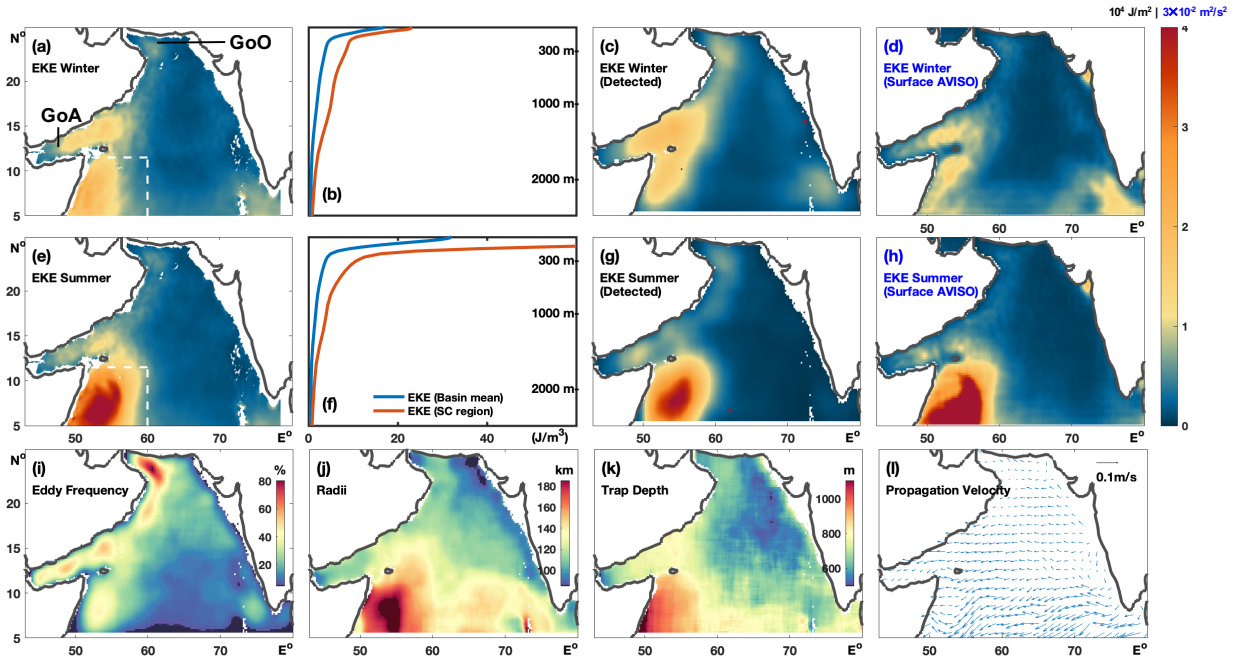
Figure 1. Distribution of energy quantities in winter (upper panel) and summer (middle panel): (a/e) vertically integrated $EKE(\frac{1}{2}\rho(u'^2 + v'^2))$, (b/f) vertically averaged EKE profile of basin (blue) and SC region (red, defined in a and e), (c/g) vertically integrated EKE estimated from detected eddies, (d/h) surface $EKE(\frac{1}{2}\rho(u'^2 + v'^2))$ estimated from AVISO altimetry data. The arrows in (b/f) depict the vertically averaged velocity in winter/summer. Distribution of detected eddies properties: (i) eddy frequency, (j) eddy radius, (k) eddy trap depth, (l) eddy propagation speed.
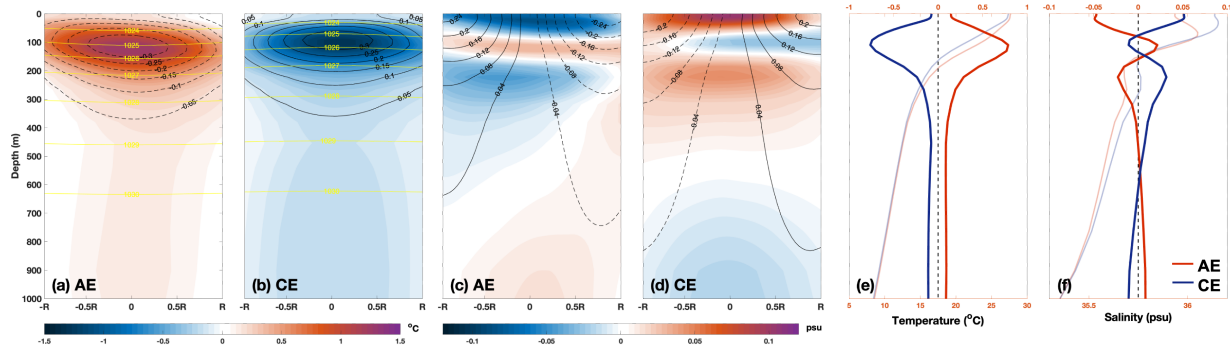
Figure 2. Composite zonal sections of vertical structure across the anticyclonic eddy (a, c) and cyclonic eddy (b, d). In (a, b), the composite temperature anomaly, density anomaly, mean density are depicted with color shading, black dotted line and yellow solid line, respectively. In (c, d) the composite salinity anomaly, positive meridional (northward) velocity, negative meridional (southward) velocity are depicted with color shading, black solid line and black dotted line, respectively. Averaged profiles of temperature (e) and salinity (f) within AE (red) and CE (blue), where dark and light lines depict anomalies and mean values, respectively.
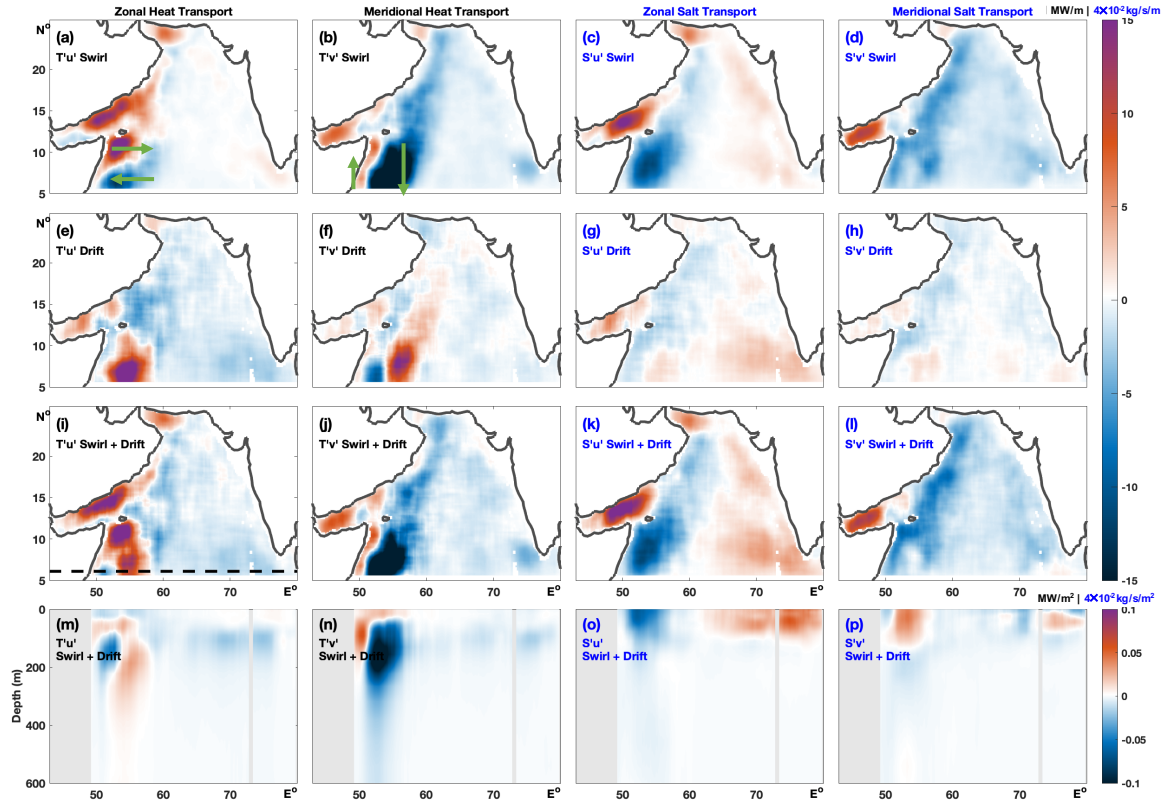
Figure 3. Distribution of vertically integrated eddy-induced transport, the left to right columns illustrate zonal heat transport, meridional heat transport, zonal salt transport and meridional salt transport, respectively. The 1st (a-d), 2nd (e-h), and 3rd (i-l) rows show eddy swirl transport due to rotation, eddy drift transport due to propagation, and total transport, respectively. The bottom row (m-p) shows the corresponding vertical distribution of total transport at the cross section of $8\,°N$ indicated by the dotted black line in (i).
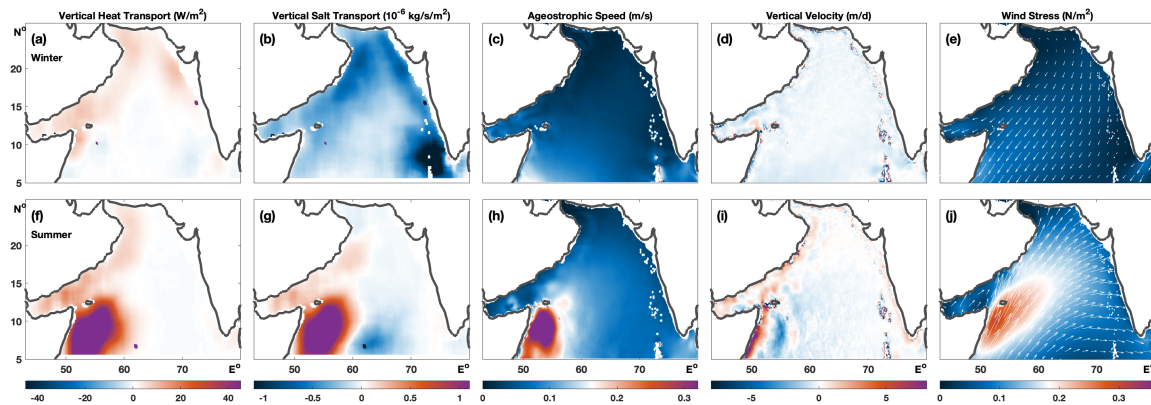
Figure 4.   Eddy-induced vertical transport of heat (a and f) and salt (b and g), magnitude of ageostrophic velocity (c and h), and magnitude of vertical velocity (d and i) at the depth of 50 m. This depth is chosen within which the ocean is almost always well mixed. Surface wind stress (e and j) in arrows and their magnitude in color. The upper and lower panels represent the distributions in averaged in winter and summer, respectively.
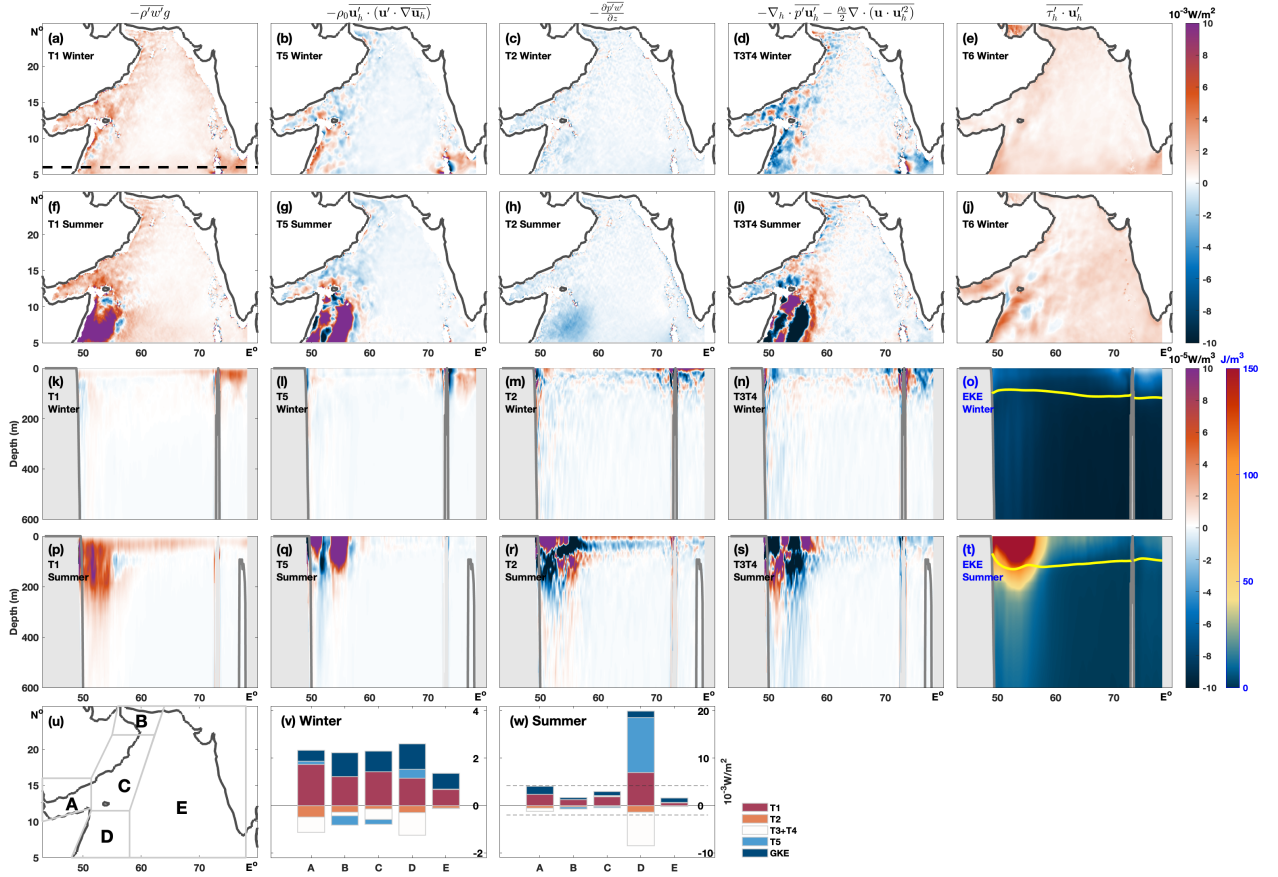
Figure 5. Eddy energy flux terms ($-\overline{\rho'w'}g$ (T1), $-\rho_0\overline{\mathbf{u}'_h \cdot (\mathbf{u}' \cdot \nabla\overline{\mathbf{u}_h})}$ (T5), $-\frac{\partial\overline{p'w'}}{\partial z}$ (T2), $-\nabla_h \cdot \overline{p'\mathbf{u}'_h} - \frac{\rho_0}{2}\nabla \cdot \overline{(\mathbf{u} \cdot \mathbf{u}'^2_h)}$ (T3T4)) integrated in the upper $1200\ m$ averaged for winter (a-d) and summer (f-j), and the corresponding vertical structure along the cross section marked by the dashed line in (a) for winter (k-n) and summer (o-r). Distribution of generation of EKE due to surface power input by time-varying wind ($\overline{\mathbf{u}'_h \cdot \tau'_h}$) in winter (e) and summer (j). Vertical structure of EKE along the cross section in winter (o) and summer (t), where the yellow solid lines depict the isopycnic of $1025\ kg/m^3$. Five sub-regions (u) of the AS and the corresponding domain averaged EKE flux terms in winter (v) and summer (w).